Propeller Performance Measurements at Low Reynolds Numbers

Silvestre, M.A.R., Morgado, J., Alves, P., Santos, P., Gamboa, P., and Páscoa, J.C.

***Abstract*—** Propellers are being used as propulsive devices since the early days of aviation. However, if they are not properly designed, they can have poor efficiency, especially at low Reynolds numbers environments such as the case of the high altitude airships envisioned in the MAAT project. Experimental data those operating conditions are crucial to effectively improve and validate new numerical design tools. This work presents the development of an experimental setup for low Reynolds propeller testing. The experimental data were successfully compared against reference data to validate the test rig. In addition, the performance data for commercially available propellers that were not characterized in the existing literature is also presented.

***Keywords*—** Airships, Low Reynolds Propellers, MAAT Project, Wind Tunnel Experiments.

I. Introduction

IN the last years, high-altitude airships have been considered as a platform for different purposes [1]. Particularly, for application as telecommunication platforms, surveillance, monitoring and for transportation of people and goods [2-8]. In Europe, the Multibody Concept for Advanced Airship for Transport (MAAT [9]) airships are being developed as an alternative medium and long range transportation system. The project involves 12 different institutions and aims to develop a heavy lift cruiser–feeder airship system. Since the cruiser will operate at stratospheric altitudes, propellers are a valid option for propulsion [6,10-16].

Due to the high altitudes the MAAT airship propellers will operate in a Low Reynolds Number (LRN) flow environment. LRN effects can decrease the performance of propellers and the ability of the available numerical methods to predict that performance. To deal with this, JBLADE [17] software is being developed, as an open-source propeller design code, using a modified [18] Blade Element Momentum (BEM) theory which accounts for three dimensional flow equilibrium. The software is coupled with XFOIL [19, 20]for its suitability in predicting LRN airfoil performance [21] JBLADE will be used to design different propellers as well as to estimate their off-design performance.

To improve the prediction capability of JBLADE, accurate LRN propeller performance data is needed.

Experimental work on propeller performance was abundant before WWII [22, 23] and a sound database of propeller performance characteristics got established. That was the golden age of propeller driven aircraft. After WWII, the widespread of jet propulsion [24] limited the use of propellers to light aircraft. However, in recent times, the small Unmanned Aerial Vehicles (UAV) advent has triggered the interest in the LRN wing and propeller aerodynamics. UIUC Applied Aerodynamics Group is a world leading institution, very active in the study of LRN aerofoils and propellers, with several publications describing experimental studies on propeller performance [25-28].

This paper describes the development of a test rig for measuring propeller performance and the experimental tests procedure simulating the LRN environment found at high altitudes. A number of wind tunnel tests performed on different small propellers is reported. In addition, the validation of the experiments is described in detail and performance data not found in the literature is presented for a couple of well-known commercial propellers.

II. Methodology

A. Experimental Setup

The design chosen for the propeller thrust balance closely resembles the T-shaped pendulum concept implemented by UIUC [25]. A sketch of the design is shown in Fig. 1. An effort was made to reduce the complexity of the assembly inside the wind tunnel, in order to ensure minimal flow and measuring disturbances. The T-shaped pendulum is pivoted about two flexural pivots while being constrained by a load cell outside of the tunnel in an area above the test volume, where plenty of room is available. The flexural pivots are frictionless, stiction-free bearings with negligible hysteresis that are suited for applications with limited angular travel. The pivots are made with flat, crossed flat springs that support rotating sleeves. These flexural pivots were chosen over the standard bearings since they greatly reduce the adverse tendencies that bearings are prone to, when used in static applications, namely stiction and hysteresis.

M. A. R. Silvestre is with the Aerospace Sciences Department of University of Beira Interior, Edifício II das Engenharias, Calçada Fonte do Lameiro, n.º 1, 6201-001 Covilhã, Portugal (corresponding author, phone: +351 275 329 732 e-mail: mars@ubi.pt).

J. Morgado is with the Aerospace Sciences Department of University of Beira Interior, Covilhã, Portugal.

P. Alves is with the Aerospace Sciences Department of University of Beira Interior, Covilhã, Portugal.

P. Santos is with the Aerospace Sciences Department of University of Beira Interior, Covilhã, Portugal.

P. Gamboa is with the Aerospace Sciences Department of University of Beira Interior, Covilhã, Portugal.

J. C. Páscoa is with Electromechanics Department of University of Beira Interior, Covilhã, Portugal.

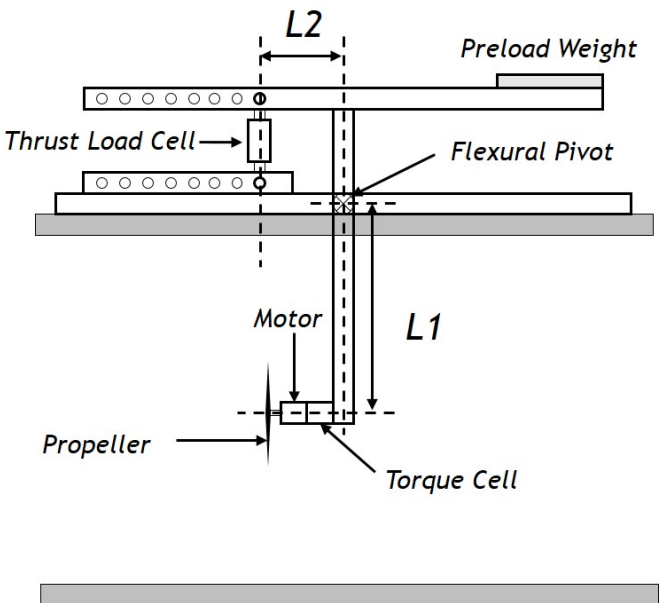

Fig. 1 T-shaped pendulum thrust balance concept.

The pendulum was designed in order to have the thrust vector located at the center of the test section. Another design concern was to ensure that there would be enough space for assembling the load cell and its accessories above the wind tunnel upper wall. Due to the 0.8mX0.8m dimensions of the test cross-section, it was decided to limit the maximum diameter of the propellers that can be tested to 14". Using the data available at the propeller performance database provided by UIUC [28], it was concluded that for 14" propellers, in static conditions, the worst case scenario, the maximum measured thrust is close to 15N.

A preload weight was added to the balance on the opposite side to the load cell (see Fig. 2). This preload weight keeps the load cell in tension throughout propeller testing to make sure the load cell does not slip during negative thrust conditions.

Load Cell Variable Positioning

One of the key concepts for the assembly's sensitivity is the possibility to adjust the position of the load cell along the upper arm of the pendulum. Thus, it becomes possible to use the full range of the load cell for different intervals of propeller's produced thrust. Fig. 2 shows the system sketch, such that the distance *L2* can be adjusted between 80*mm* and 350*mm* in 10 increments of 30*mm* each.

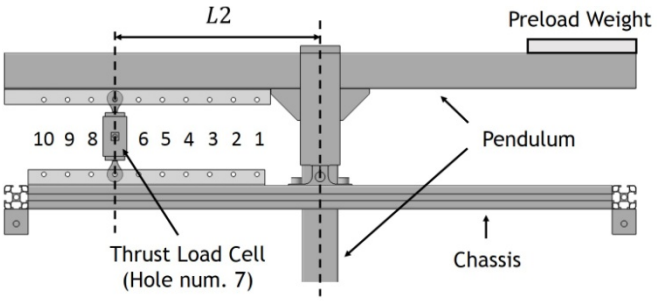

Fig. 2 Illustration of different load cell positions.

Thrust and Torq ue Measurement

The thrust load cell used is the FN3148 manufactured by FGP Sensors & Instrumentation having a maximum capacity of 100N. The torque produced by the propeller is measured using the RTS-100 and RTS-200 reaction torque transducers made by Transducer Techniques according to the torque level of the propeller being tested. Both thrust and torque load cells are connected to a high-precision strain gauge converter from mantracourt, model SCB-68 that converts a strain gauge sensor input to a digital serial output.

Propeller Speed Measurement

To measure the propeller rotation speed, a Fairchild Semiconductor QRD1114 photo-reflector was used to count the number of revolutions the output shaft makes in a fixed time interval (0.75*s*), resulting on an accuracy of ±0.5*Rev*/0.75*s*. This sensor is constituted by two distinct parts: an infrared emitting diode and a phototransistor. A simple circuit composed by a limiting resistor, a bias resistor and a *Schmitt trigger* is used. The former is used, as the name suggests, to limit the current to the infrared diode. The bias resistor is used to produce an output on the phototransistor side. The output of the phototransistor is further cleaned and digitized using a *Schmitt trigger*. The latter component is essential in order to make the output relatively independent of the distance from the reflecting surface.

Using this circuit, the sensor can be placed up to 2*mm* away from the reflective surface. The output voltage is near 0.27*V* when aimed at a white surface and about 4.61*V* when pointed at a black surface. The circuit has a response time of around 50μs. The output voltages and response time of the circuit proved to be more than sufficient for measuring the rotational speed of the propellers, which never exceeded 7000 *RPM* as shown in *Section III.*

Freestream Velocity Measurement

The freestream velocity is measured with a differential pressure transducer, an absolute pressure transducer, and a thermocouple. The measuring mechanism uses two static pressure ports, one at the tunnel settling section and another at the entrance of the test volume, as it presented in Fig. 3.

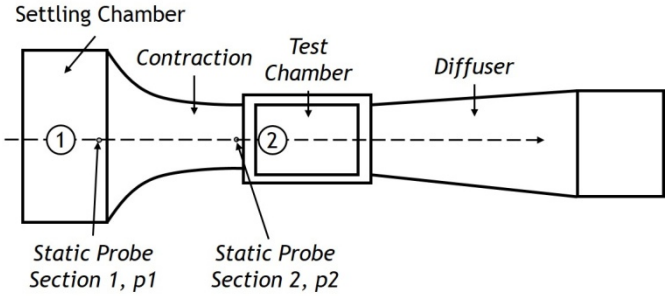

Fig. 3 Location of the static pressure ports.

The contraction section makes the velocity increase and the pressure decrease at the test chamber. This pressure

difference is a measure of the tunnel flow rate. Thus, the velocity can be determined from Bernoulli's equation:

$$\frac{p_1}{\rho}+\frac{1}{2}V_1^2+gz_1=\frac{p_2}{\rho}+\frac{1}{2}V_2^2+gz_2 \quad (1)$$

Considering that the tunnel is horizontal, $z_1 = z_2$, then:

$$V_2^2-V_1^2=\frac{2(p_1-p_2)}{\rho} \quad (2)$$

The incompressible continuity relationship:

$$A_1V_1=A_2V_2 \quad (3)$$

or

$$V_1=\frac{A_2}{A_1}V_2 \quad (4)$$

Combining (2) and (4), allows the determination of the flow velocity in the test section:

$$V_2=\sqrt{\frac{2(p_1-p_2)}{\rho\left[1-\left(\frac{A_2}{A_1}\right)^2\right]}} \quad (5)$$

The atmospheric pressure outside of the tunnel is measured with the absolute pressure transducer model MPXA4115A made by Freescale Semiconductor. The temperature is measured with a National Instruments LM335 thermocouple located at the inlet of the wind tunnel. This measuring method is also independent of possible inaccurate installations regarding the correct direction of the pitot probe as it uses the factory pre-installed wind tunnel static pressure ports.

B. Balance Calibration

Before using the rig for any tests, each measuring instrument was calibrated. The thrust calibration was made *in situ* using calibrated weights and a low-friction pulley system to create an axial load simulating the propeller thrust on the load cell (see Fig. 4 (b)). By increasing and decreasing a known force on the load cell, a linear relationship between the thrust and voltage was determined. Regarding torque sensor calibration (see Fig. 4 (a)), the calibrated weights are used with a moment arm to create a known torque, and by adding and removing weights, a linear relationship between the torque and voltage was also calculated. These calibration procedures need to be regularly performed to ensure consistent results. Calibration was later verified using check-loads. Pure and combined check-loads were repeatedly applied to verify the balance calibration.

(a) (b)

Fig. 4 Pictures of the thrust balance calibration procedure: (a) torque sensor (b) thrust load cell

C. Propeller Performance Parameters

Variables can be divided into two categories, namely measured and calculated variables. The measured variables are directly obtained from the measurement instruments. Physical measurements of thrust, torque, rotational speed, static pressures, atmospheric pressure, and temperature are gathered. From these quantities, propeller power and air density are calculated, respectively, according to:

$$P=2\pi nQ \quad (6)$$

$$\rho=\frac{P_{abs}}{RT_{atm}} \quad (7)$$

The above measured and derived quantities are non-dimensionalized in order to obtain the propeller performance characteristics. These quantities include the thrust coefficient C_T, power coefficient, C_P, and propeller efficiency, η. In the static case, since the advance ratio is zero, C_T and C_P are plotted against the propeller rotational speed. For the non-static case, the coefficients and the efficiency are plotted against the advance ratio. The definitions for the advance ratio, thrust and power coefficients, and propeller efficiency are, respectively, given by:

$$J=\frac{V}{nD} \quad (8)$$

$$C_T=\frac{T}{\rho n^2D^4} \quad (9)$$

$$C_P=\frac{P}{\rho n^3D^5} \quad (10)$$

$$\eta=J\frac{C_T}{C_P} \quad (11)$$

where, V is the freestream velocity; D is the propeller diameter; T is the propeller thrust; P is the propeller power and n is the propeller rotational speed expressed in *rot/s.*

D. Wind Tunnel Corrections

Boundary Corrections for Propellers

The interference experienced by a propeller in a wind tunnel was object of study by Glauert [29]. A propeller, when producing a positive thrust, creates a wake or slipstream of increased velocity. Considering that in a closed wind tunnel the flow is confined between solid walls, the condition of flow continuity leads to reduced velocity and increased pressure of the fluid surrounding the wake.

These modified conditions behind the propeller change the relationship between the thrust and the freestream velocity of the wind tunnel propeller for a given rotational speed. Such that, in confined conditions, the thrust developed by the propeller is greater than would be developed in an unrestricted flow of the same freestream velocity with the same propeller rotation rate and blade pitch. Or, it can also be said that the thrust developed would be equal to that which would be expected at a lower V' in freestream velocity [30]. The correction for this effect is:

$$\frac{V'}{V} = 1 - \frac{\tau_4 \alpha_1}{2\sqrt{1+2\tau_4}} \tag{12}$$

where

$$\tau_4 = \frac{T}{\rho A V^2} \tag{13}$$

and

$$\alpha_1 = \frac{A}{C} \tag{14}$$

where A is the propeller disk area and C is the jet cross-sectional area, and T is thrust.

Motor Fixture Drag

Due to the presence of the torque transducer and the motor fixture, the measured thrust is actually given by (T-$D_{fixture}$). To obtain the actual values of thrust, an assembly's drag model was implemented in order to correct the measured thrust values for different freestream velocities. The propeller thrust is, thus, given by:

$$T = \rho n^2 D^4 C_T + D_{fixture} \tag{15}$$

The assembly's drag is estimated using:

$$T = \rho n^2 D^4 C_T + D_{fixture} \tag{16}$$

with

$$q = \frac{1}{2}\rho V_{drag}^2 \tag{17}$$

Considering that the fixture is located in the propeller slipstream, a fixture drag velocity was used as the corrected freestream velocity given by Glauert's method 2.14 plus the slipstream induced velocity, at the propeller disk, given by the Actuator Disk Theory.

$$V_{drag} = -\frac{V'}{2} + \sqrt{\left(\frac{V'}{2}\right)^2 + \frac{T}{2\rho A}} + V' \tag{18}$$

E. Test Methodology

For static performance tests, the propeller thrust and torque were measured along with the local atmospheric pressure and temperature at different *RPM*. For the performance tests with freestream speed, the propeller rotational speed was set to a desired value and the wind tunnel's freestream velocity was increased from 4 *m/s* to 28 *m/s* by 1 *m/s* increments. At freestream velocities smaller than 4 *m/s*, it was difficult to obtain the needed freestream velocity stability to proceed with the measurements, due to the interference between the propeller wake and the wind tunnel's fan. At each measured freestream velocity, the propeller thrust and torque were measured along with the ambient pressure and temperature. If the torque value became too close to zero, the test was finished because the propeller was entering the windmill brake state.

The collecting data procedure (see Fig. 5) begins with the execution of the LabView® data acquisition and reduction software. This is followed by putting the program to run test condition. The control software powers up the motor to the first pre-defined RPM setting and data for each freestream velocity step is collected. This procedure was repeated for all $RPMs$. Once the data was collected, the data reduction sub-routine is executed. The collected data is systematically reduced, recorded and stored. Due to the complete automation of the process, the overall time for an entire run is just the physical tunnel run time. The procedure of collecting data in each freestream velocity is preceded by a "data convergence period" of 50s within a minimum error margin from the intended defined RPM and freetream velocity values to achieve the steady state.

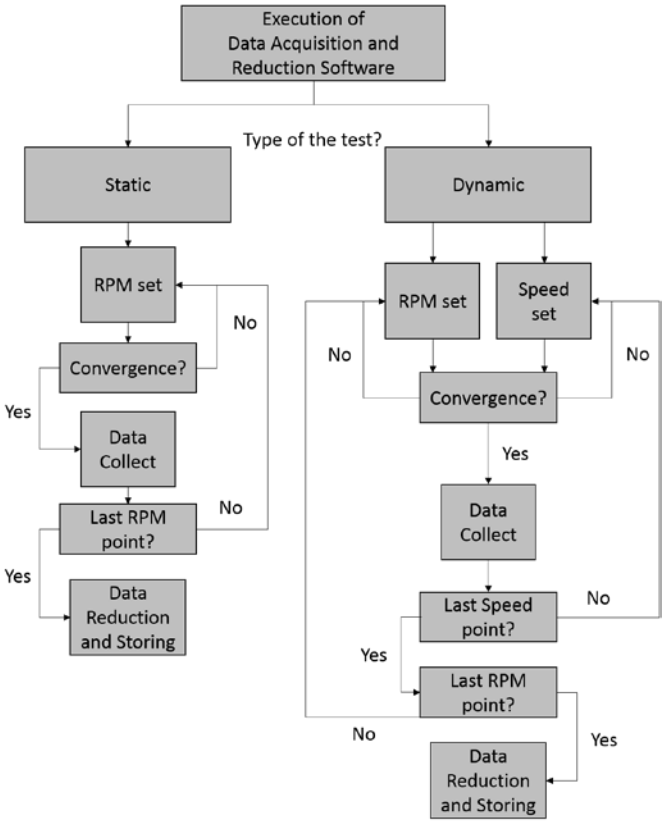

Fig. 5 Flowchart of the test methodology.

Convergence Criteria

The procedure of collecting data in each freestream velocity is preceded by a "data convergence period" to achieve the

steady state. Two similar convergence criteria are implemented, one for the freestream velocity set and the other for the propeller's RPM. Both convergence criteria are presented in Table 1:

Table 1 – Convergence criteria for *U* and *RPM*.

Criteria	Min. Time [s]
$\lvert RPM - RPM_{target} \rvert \leq 10\ RPM$	40.0
$\lvert U - U_{target} \rvert \leq 6\ m/s$	40.0

When both convergence criteria are verified, the data samples are recorded over a pre-defined period of time. In Fig. 6 an example is presented of the torque and thrust outputs during the convergence and data collect phases.

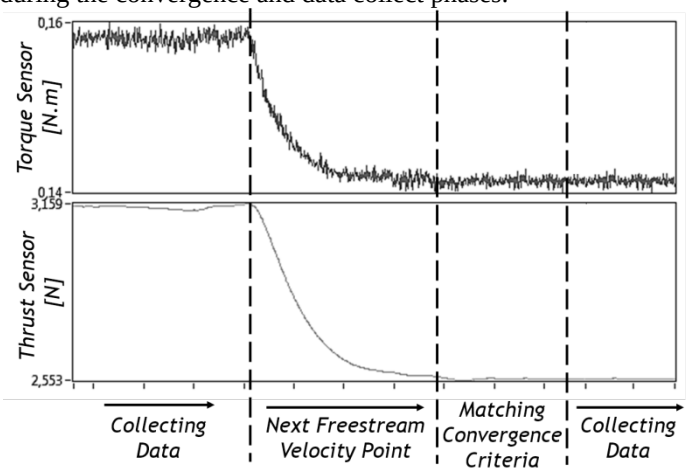

Fig. 6 Torque and Thrust outputs during the convergence and data collection phases.

III. Validation of the Test Rig

Before performing tests for new and uncatalogued propellers, the test rig was submitted to a complete validation study. The validation included a sample independence test in order to ensure that the results are not affected by the number of samples used to collect each point. The same propeller test was run with five different sampling settings as presented in Section 3.1. In addition, to ensure the repeatability of the measurements, the same propeller was tested in 3 different days, as shown in Section 3.2. Furthermore, the propeller performance obtained in UBI's wind tunnel was compared with the data obtained by UIUC[31].

A. Sampling Independence

The recorded output value of any measured or calculated variable is a mean of *N* values recorded at a sample rate of 8*Hz*. Since this frequency is constant, when the sample number, *N*, increases, the sampling time also increases and the test runtime becomes higher. This validation test was performed in order to find an acceptable samples number that does not affect the final result. The APC 11"x5.5" Thin Electric propeller was used.

Table 2 No. of samples vs sampling time.

Number of Samples, *N*	Sampling Time, *s*
50	6.25
100	12.5
200	25.0
400	50.0
800	100.0

The results presented in Fig. 7 show some discrepancies for an advance ratio around 0.3 for the lower number of samples used to collect the data (50 and 100 samples) but converge for *N*>200. To ensure a correct data collection, 400 samples setting was used in all the tests presented herein. That with the 8 *Hz* sampling rate made each point collecting phase takes less than one minute.

B. Measurements Repeatability

To ensure that the measurements are not dependent on the weather conditions on a specific day, the measurements for a specific propeller were performed on 3 distinct days. Furthermore, the measurements repeatability quality is an indicator of the integrity of the measurement system. If a measurement system cannot produce consistent and repeatable measurements, a verification of the measurements accuracy cannot be performed. The test rig was submitted to repeatability tests fulfilling the following conditions:

- The same propeller and the same measurement procedure;
- The same measuring instruments, used under the same conditions;
- The same instrument calibration;
- Repetition over 3 consecutive days.

Fig. 8 shows comparisons of the APC 11"x5.5" Thin Electric performance data collected for the repeatability tests. Although the tests were performed during the summer, the weather conditions were quite different in the three days of testing, with sun on the first day moving to wind and rain on the remaining two days. However, the plotted results show an exceptional repeatability for all the performance parameters.

C. Performance Data Comparison

Two different APC commercial propellers were chosen to this step of validation, the 10x4.7" Slow Flyer and the 11x5.5" Thin Electric. Its performance data was compared with data available in the literature. The data for comparison was downloaded from the UIUC Propeller Data Site [28] and corrected according to Ref. [32].

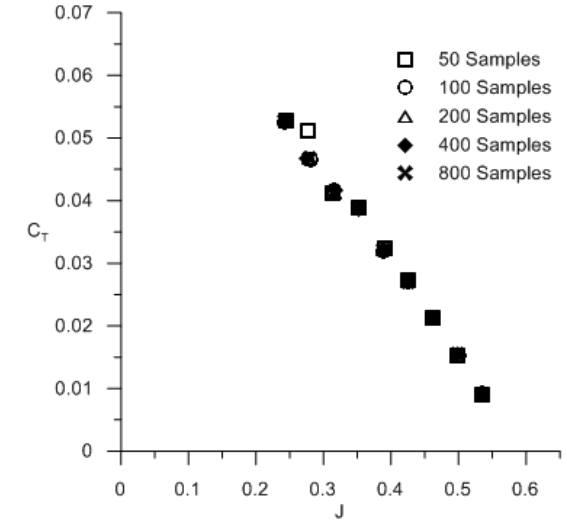

(a)

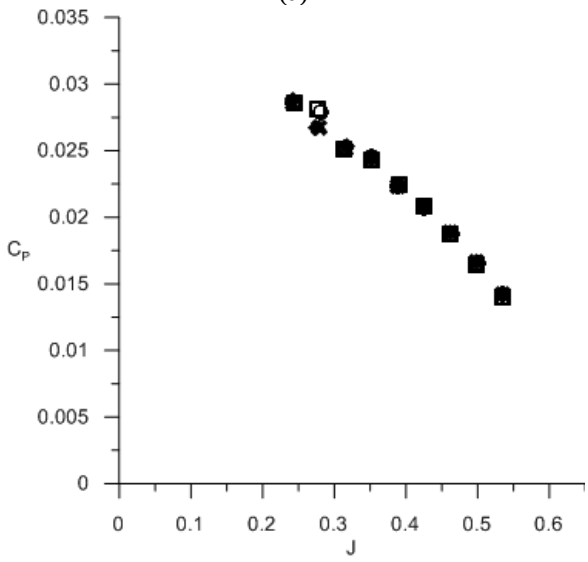

(b)

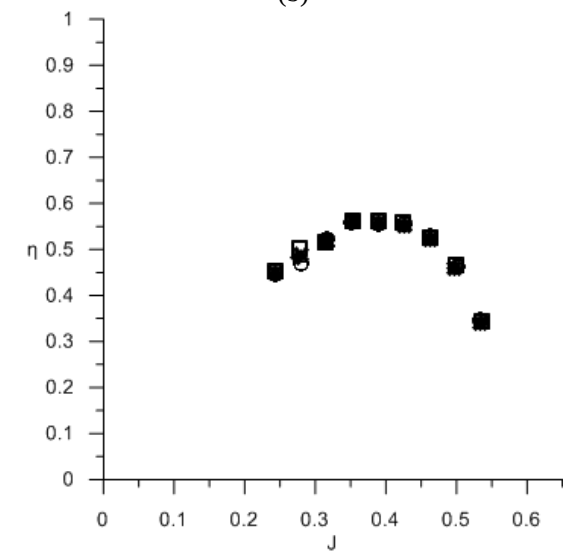

(c)

Fig. 7 Comparison using different number of samples for an APC 11”x5.5”. (a) thrust coefficient (b) power coefficient (c) propeller efficiency.

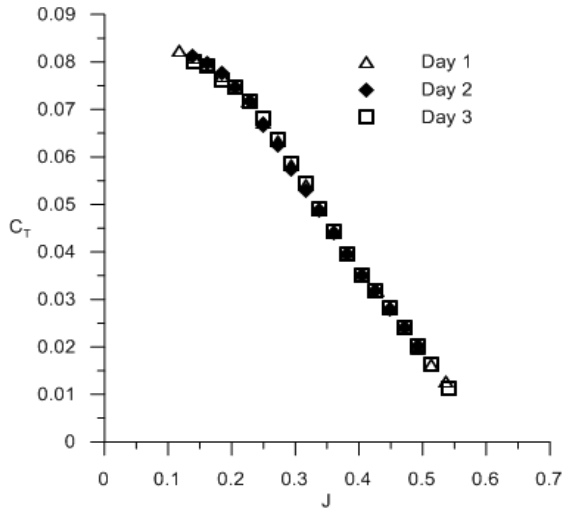

(a)

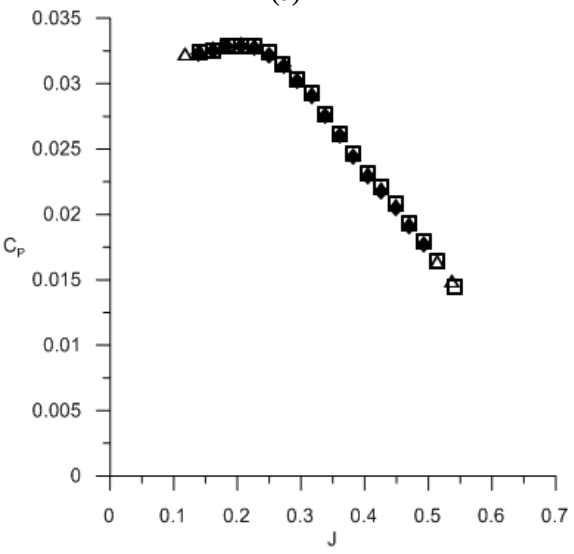

(b)

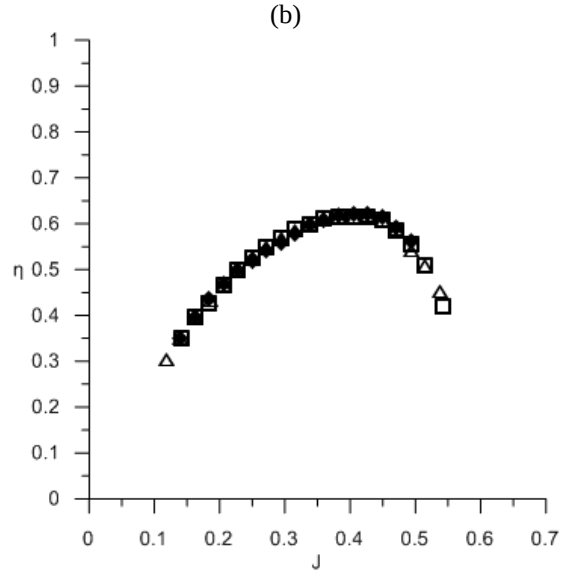

(c)

Fig. 8 Comparison of measurements performed in 3 different days. (a) thrust coefficient (b) power coefficient (c) propeller efficiency.

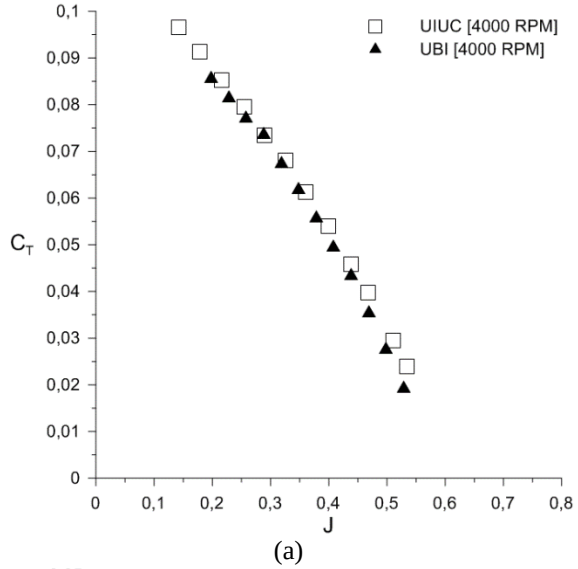

(a)

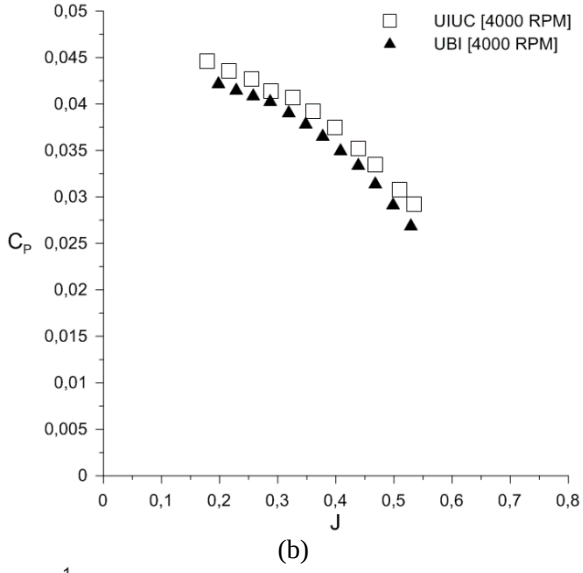

(b)

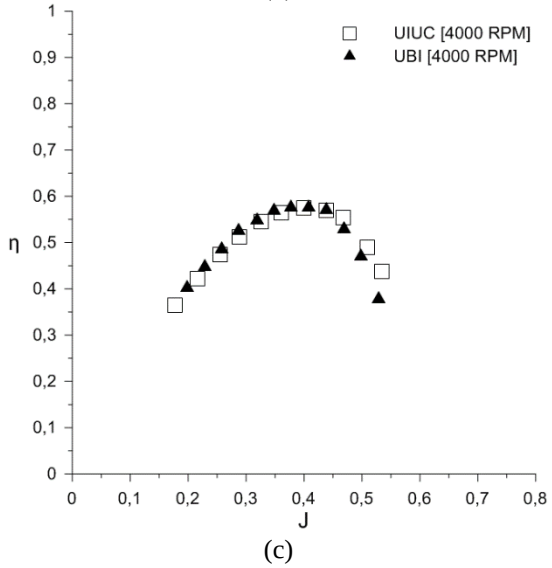

(c)

Fig. 9 APC 10”x4.7” Propeller data for 4000 *RPM* (a) thrust coefficient (b) power coefficient (c) propeller efficiency.

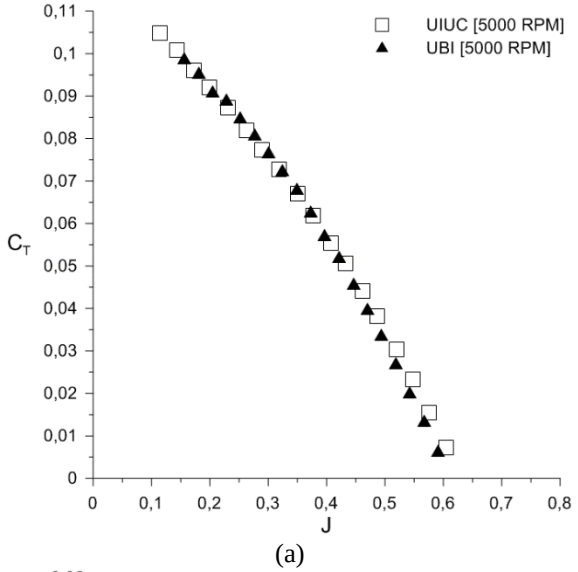

(a)

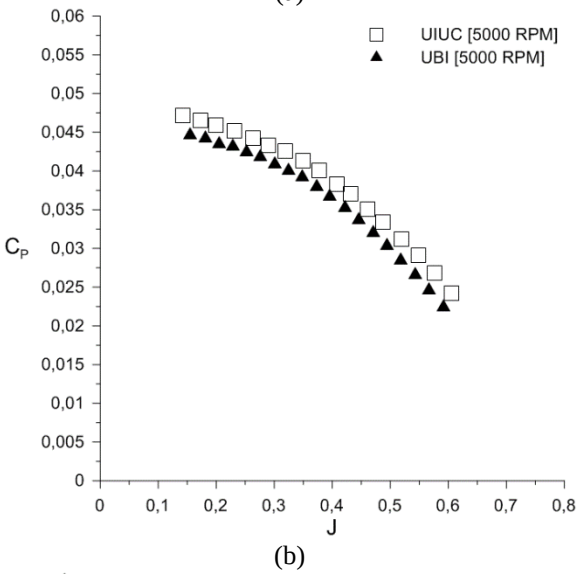

(b)

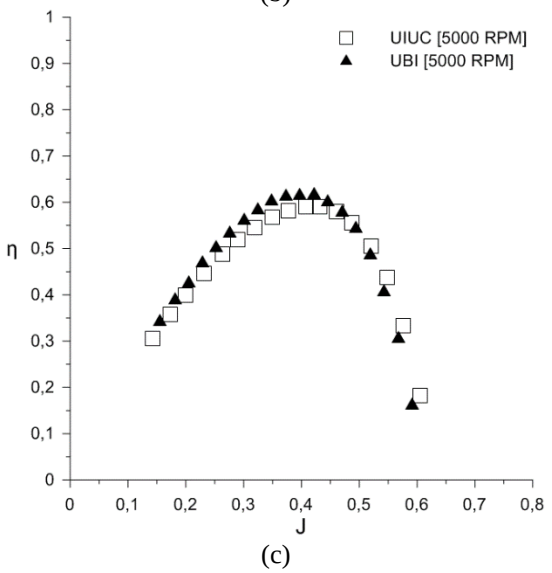

(c)

Fig. 10 APC 10”x4.7” Propeller data for 5000 *RPM*. (a) thrust coefficient (b) power coefficient (c) propeller efficiency.

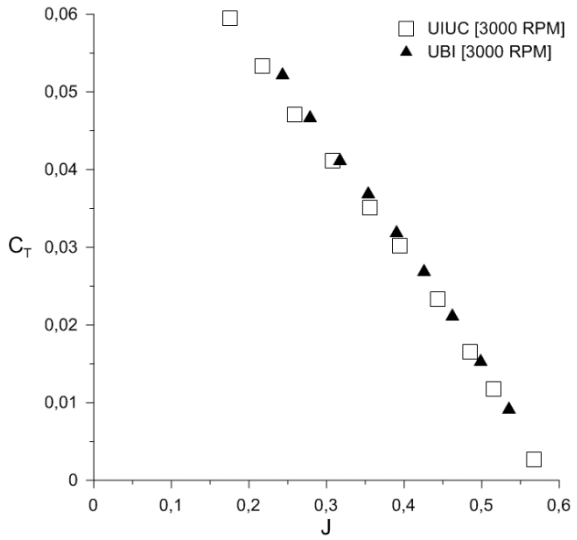

(a)

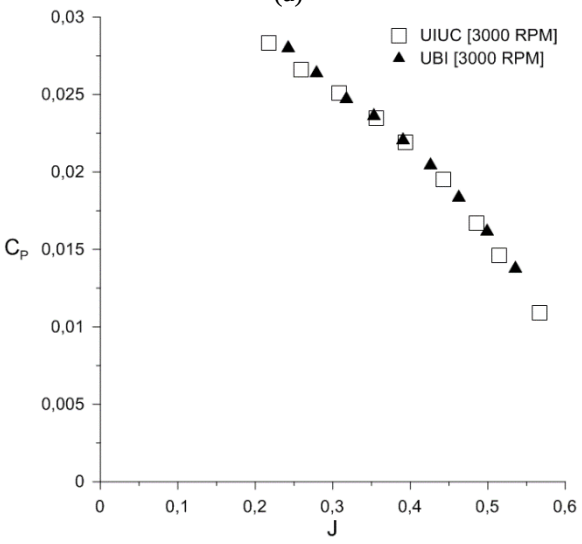

(b)

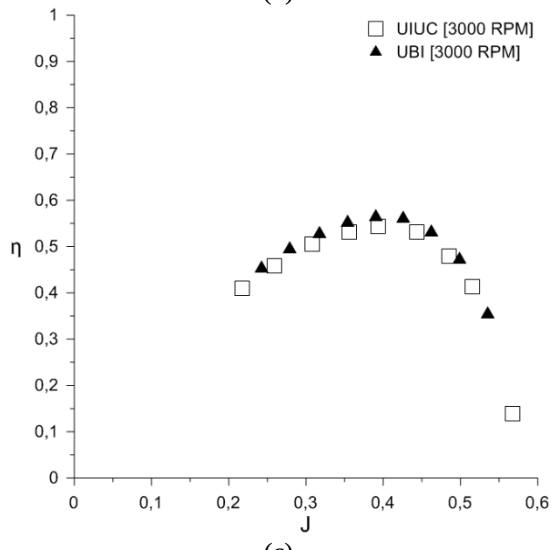

(c)

Fig. 11 APC 11”x5.5” Propeller data for 3000 *RPM*. (a) thrust coefficient (b) power coefficient (c) propeller efficiency.

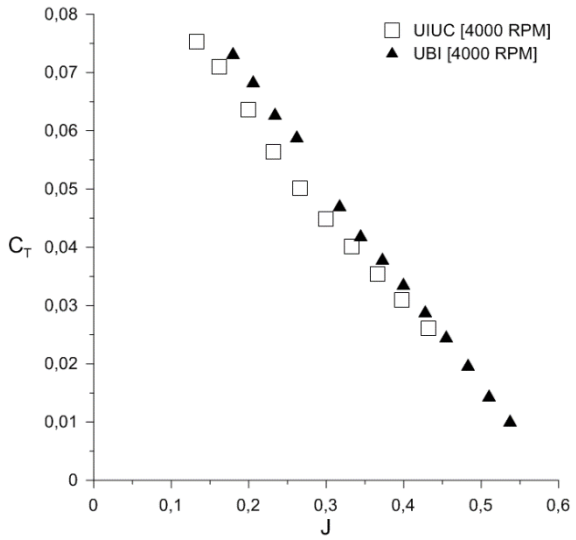

(a)

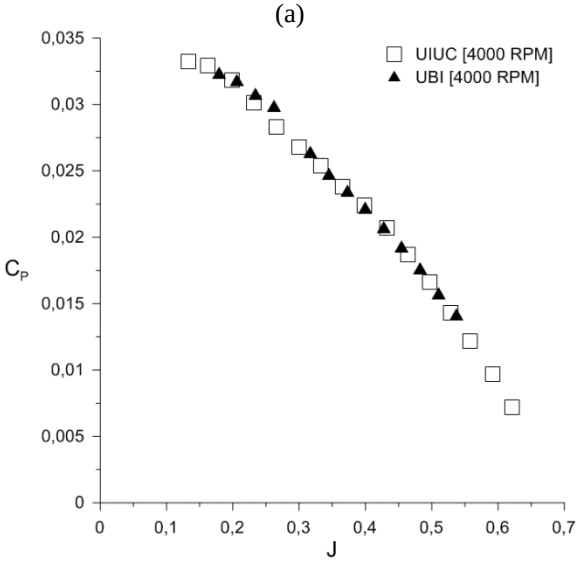

(b)

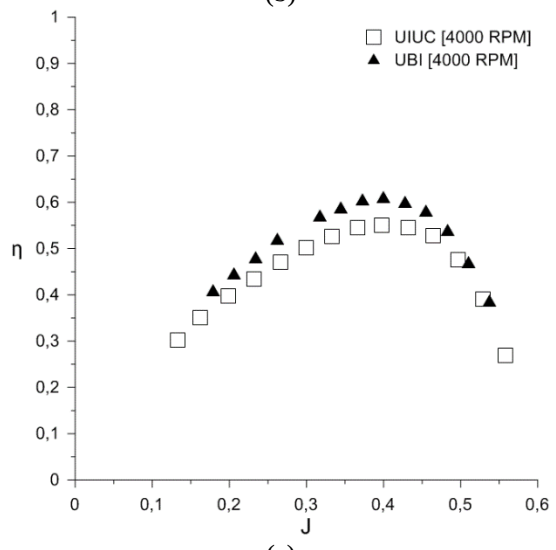

(c)

Fig. 12 APC 11”x5.5” Propeller data for 4000 *RPM*. (a) thrust coefficient (b) power coefficient (c) propeller efficiency.

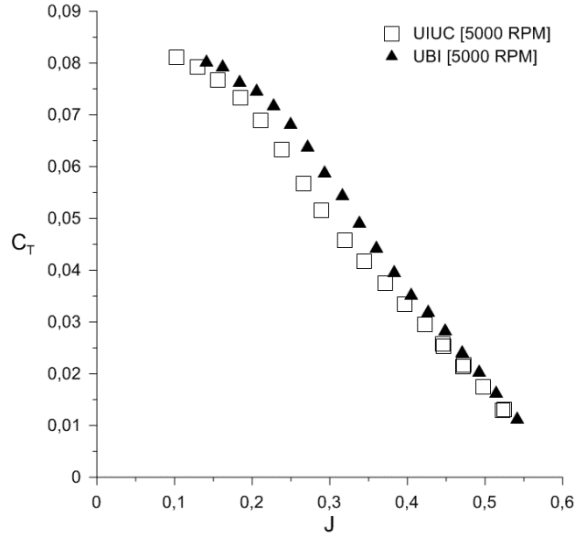

(a)

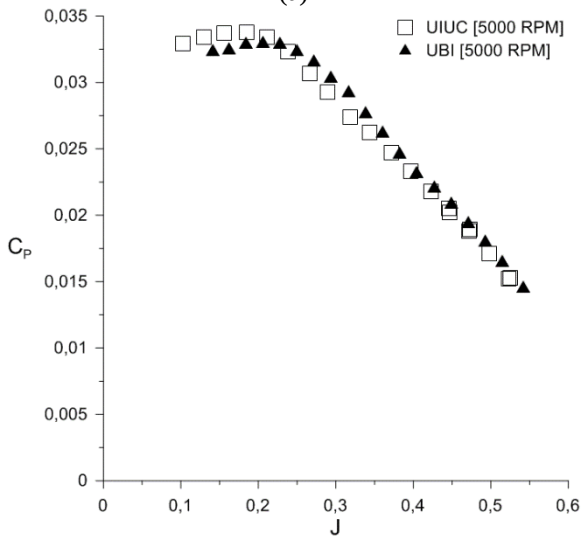

(b)

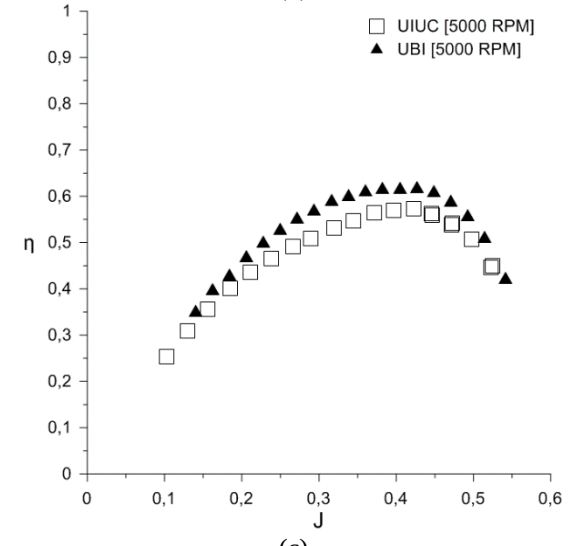

(c)

Fig. 13 APC 11”x5.5” Propeller data for 5000 *RPM*. (a) thrust coefficient (b) power coefficient (c) propeller efficiency.

Analyzing the results of the 10”x4.7” Slow Flyer propeller (see Fig. 9 and Fig. 10) it is seen that for the 4000RPM the measured thrust coefficient are slightly lower than those of UIUC, on the other hand, for 5000RPM this parameter closely matches the UIUC data points. Furthermore, for both rotational speeds UBI’s coefficient of power shows a negative offset of approximately 6% comparing to UIUC. Regarding the efficiency plots for this propeller, the measured efficiency at 4000RPM was closely the same whereas for 5000RPM UBI measured a maximum higher efficiency for a slightly lower advance ratio.

Regarding the results obtained for the APC 11”x5.5” Thin Electric propeller (see Fig.11 to Fig. 13), it is possible to observe that for 3000*RPM*, the thrust coefficient from closely matches that of UIUC [28]. On the other hand, for 4000 and 5000*RPM* there is an offset on the thrust coefficient value, UBI showing a larger value. This difference is more pronounced at intermediate advance ratios. Regarding the power coefficient, the values measured by UBI are again in good agreement for 3000 and 4000*RPM* and a slight difference appears at 5000 *RPM*, with positive offset in the intermediate *J* values, gradually becoming negative towards the lower end of the advance ratio. Since the propeller efficiency is dependent on the thrust and power coefficients, the differences in thrust coefficients are also present in the propeller efficiency graph. In addition, it is possible to observe that both thrust and power coefficients increase with the increase in the propeller rotational speed. This is a typical LRN behavior and relates to the increase of the airfoil maximum lift coefficient throughout the blade at higher Reynolds number to increased rotational speed. Another airfoil characteristic that improves with the Reynolds number is the lift/drag ratio. This becomes evident observing the efficiency increase from 3000*RPM* to 5000*RPM*, where the UBI data shows a greater improvement than the UIUC data. Nevertheless, the curve trends that are a clear feature of the propeller model are alike.

The existing differences in the performance between UBI and UIUC data can be explained by the different propeller rotational speed controlling system used by UBI and UIUC. During the collecting data phase an effective rotational speed control mechanism is a key factor. There is a large coupling between the wind tunnel freestream velocity and the propeller rotational speed. So, the average propeller rotational speed value is not a representative number in terms of data accuracy in case there is significant *RPM* variance, σ. Considering the same average *RPM* value, the higher the fluctuations around the target *RPM*, the higher the power that will be consumed. As it is stated in Ref. [31], UIUC initially used a manual control of the throttle setting through the knob of a device called the ServoXciter EF. After testing this “open loop” controlling system it was observed the actual *RPM* values fluctuated up to 40 *RPM* around the target value for different freestream velocities. UBI uses a closed loop PID controller, showing maximum fluctuations of 5 *RPM* around the target *RPM* value during the data collection.

D. Propeller Performance Data

After validating the test rig, two uncatalogued propellers were tested. These propellers belong to two different UBI's Aerospace Science Department UAV projects: OLHARAPO and LEEUAV. The propeller used by OLHARAPO is a 12"x8" Aeronaut CAM Carbon Electric folding, with 3 blades. Regarding the LEEUAV, it uses a 13"x8" Aeronaut CAM Carbon Electric folding, 2-bladed propeller.

Aeronaut CAM Carbon Electric 12"x8" – 3 Blades

The results of the 3 bladed Aeronaut CAM Carbon Electric propeller are shown in Fig.14. The results show an increase in both thrust coefficient and power coefficient with an increase in the propeller *RPM*. However, since the increase in the thrust coefficient is higher than that of the power coefficient, it results in a higher propeller efficiency for higher *RPM*'s. As mentioned in Section 3.3 this is due LRN detrimental effect fading away as the Reynolds number increases with the rotational speed.

The maximum efficiency of this propeller increases from about 65% for an advance ratio of 0.55 at 3000 *RPM* to 75% at an advance ratio of 0.65 and 7000 *RPM*.

Aeronaut CAM Carbon Electric 13"x8" – 2 Blades

Results for the Aeronaut Carbon Electric 13"x8" 2 bladed propeller are shown in Fig. 15. It is possible to observe an increase in the thrust coefficient with the Reynolds number, but no significant changes are visible in the power coefficient. Consequently, the thrust increase leads to the typical increase in the LRN propeller efficiency as the Reynolds number increases with propeller *RPM*.

E. Propeller Efficiency Comparison

The four propellers subjected to the performance tests presented in this work, can be divided in two categories, namely the fine pitch propellers, including the two from APC; and the coarse pitch propellers, including the two remaining Aeronaut propellers. In order to investigate the effect of the propeller pitch on the overall efficiency, two additional charts are plotted in Fig. 16 comparing the efficiency of the four propellers at 4000 RPM and 5000 RPM respectively.

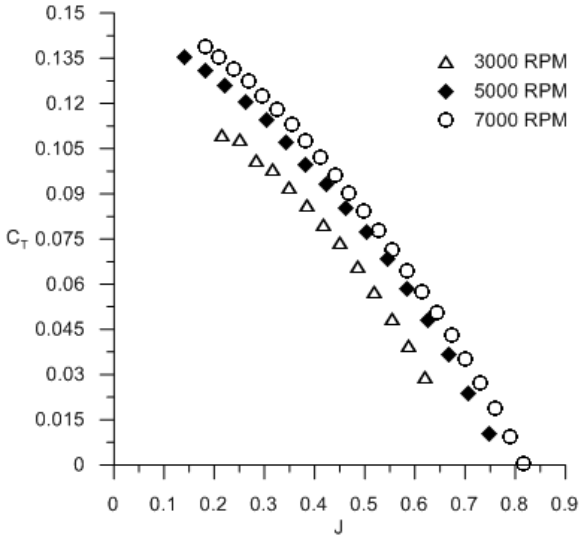

(a)

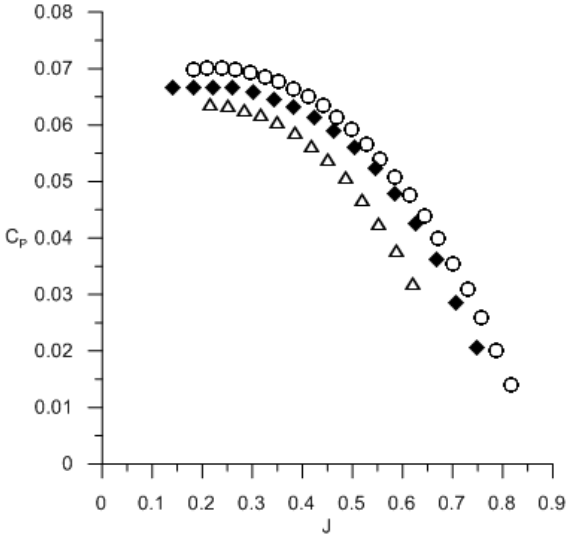

(b)

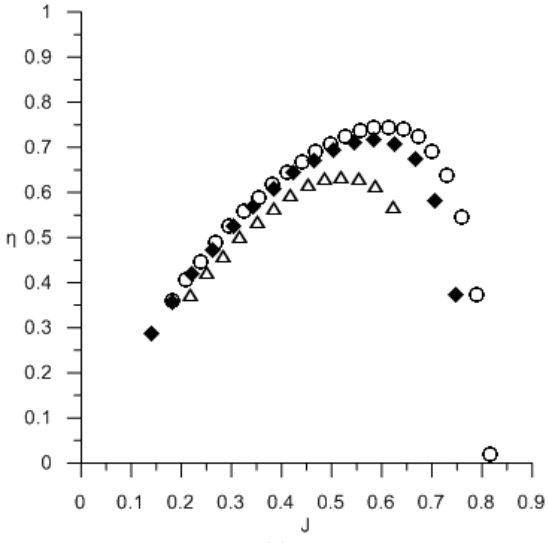

(c)

Fig. 14 Aeronaut 12x8" Propeller data for 3000 *RPM*, 5000 *RPM* and 7000 *RPM* (a) thrust coefficient (b) power coefficient (c) propeller efficiency.

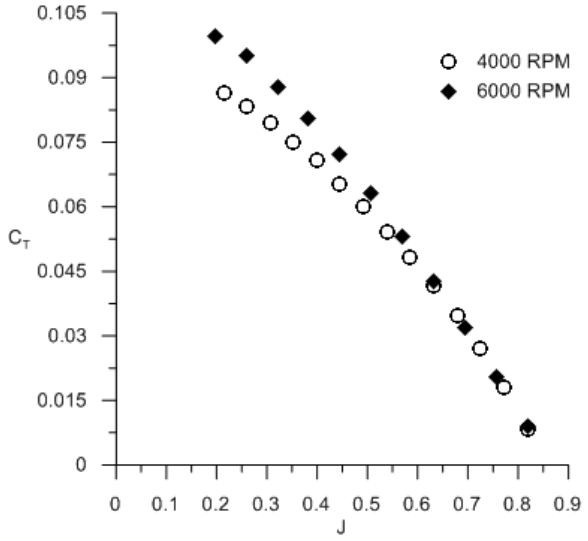

(a)

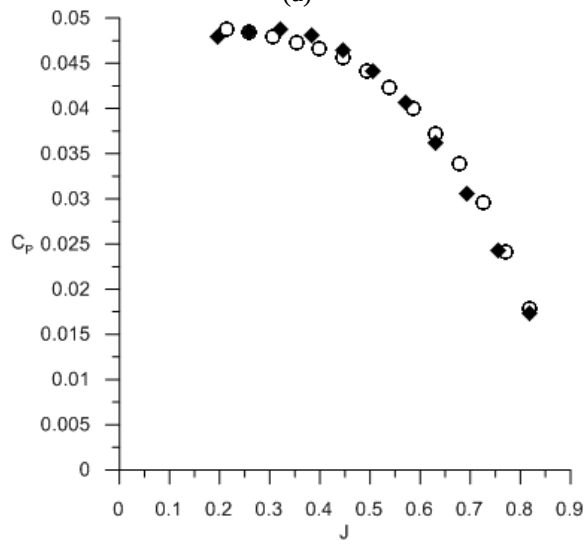

(b)

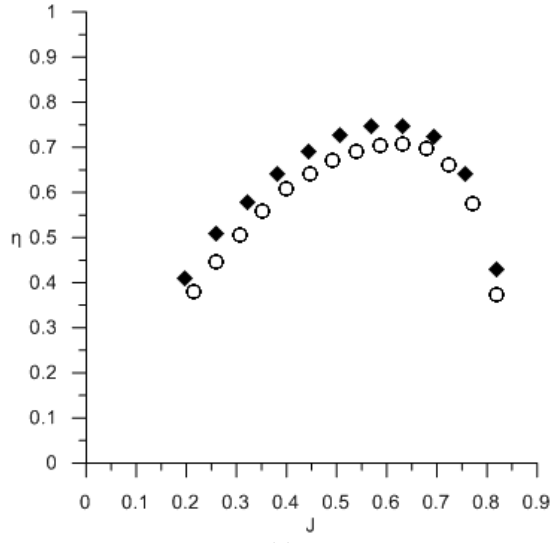

(c)

Fig. 15 Aeronaut 13"x8" Propeller data for 4000 *RPM* and 6000 *RPM* (a) thrust coefficient (b) power coefficient (c) propeller efficiency.

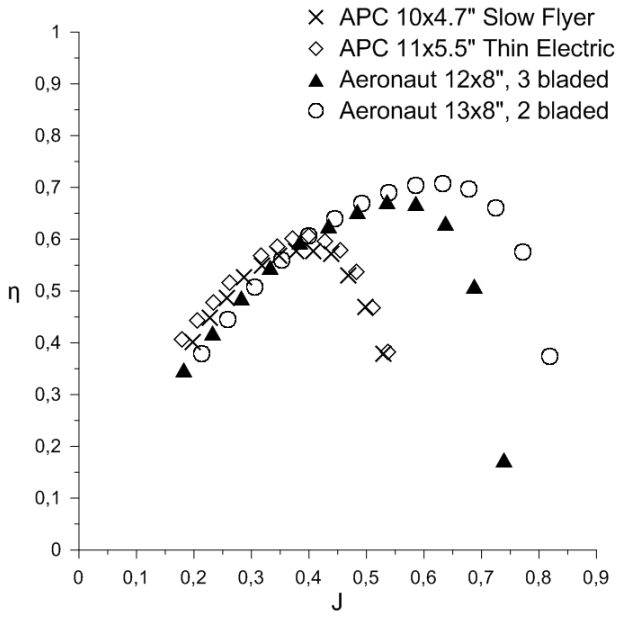

(a)

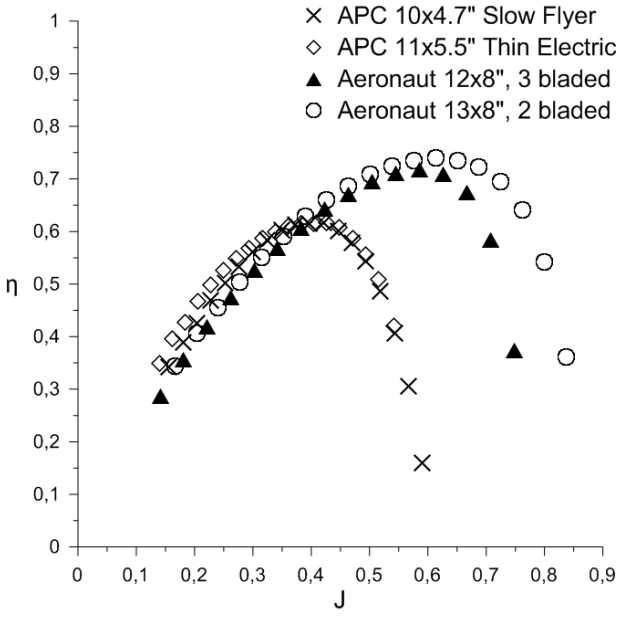

(b)

Fig. 16 Efficiency comparison of the four tested propellers. (a) 4000RPM (b) 5000RPM

Analyzing the results of the comparison between the tested propellers, it is possible to observe that:

- The two Aeronaut propellers, with their coarse pitch, have higher maximum efficiency;
- The two APC propellers shown a higher efficiency for advance ratios lower than 0.4;
- The maximum efficiency of the tested fine pitch propellers is around 60% for an advance ratio of 0.4. On the other hand, the maximum efficiency of the Aeronaut propellers is higher than 70%;
- At the maximum efficiency point of the APC propellers (*J=0.4*), there are no significant differences in the efficiency of all the tested propellers for both rotational speeds;

- Between both APC propellers, the APC 11"x5.5" Thin Electric shows to be more efficient in all presented conditions. The difference in efficiency between this two propellers appear to be more pronounced at lower RPM and may be attributed to the higher Reynolds number of the bigger propeller for a given rotational speed;
- Between both Aeronaut propellers, the 2 bladed Aeronaut 13"x8" shows to be more efficient in all presented conditions. The Aeronaut 13"x8" has a maximum efficiency of about 74% for an advance ratio of 0.6, while the 3 bladed Aeronaut 12"x8" shows a maximum efficiency of slightly above 70% for a lower advance ratio of 0.55. The difference in efficiency between this two propellers appear to be more pronounced at higher advance ratios ($J > 0.55$), this can be explained by the different number of blades between the two;

The fine pitch propellers show a smaller range of usable advance ratios (0.1 to 0.6) when compared with the coarse pitch propellers which show a wide range of operational advance ratios (0.1 to 0.85).

F. Uncertainty Analysis

The measurements error propagation begins with the primary quantities including thrust, torque, ambient pressure, ambient temperature and tunnel flow rate static ports differential pressure. The purpose of the error analysis is to determine the level of precision of the presented propeller performance results. In order to execute the analysis it was assumed that there is no error on the conversion from the sensor's voltages to the physical quantities; on the propeller diameter since it is given as a specification from the propeller manufacturer and on the wind tunnel sections dimensions since it is given as a specification from the manufacturer.7

Although the manufacturers provide this uncertainty information about the sensors, all the primary readings experience some level of fluctuations. If the fluctuations in the measurement of parameter X have a normal distribution, then 95% of the samples will fall within $\pm 2\sigma$ of the mean, so $\delta(X)=2\sigma$ can be applied [33]. The uncertainties analyzed include the wind tunnel freestream velocity, the propeller advance ratio, rotational speed, coefficients of thrust and power as well as the efficiency. A summary of the uncertainty analysis relative to the 12"x8" Aeronaut CAM Carbon folding 3-bladed propeller at 5000 *RPM* test is presented in the Table 3.

It can be noted that:

- For freestream velocities around 5-6 *m/s* interval there is an increased uncertainty in the results. By analyzing the raw data, this appears to be a result of higher fluctuations on the measurements around this velocity interval;
- For freestream velocities above 7 *m/s*, the uncertainty in this parameter is less than 1%;
- The uncertainty in C_T is typically less than 0.3%;
- The uncertainty in C_P is typically less than 0.6%;
- The uncertainty in η is typically less than 1%.

The observed uncertainties prove to be small and, as expected, they increase as the predominant primary measurement decreases such as the uncertainty in freestream velocity which increases as P_{diff} measurements decrease. This increased uncertainty can be found at the 5-6 *m/s* freestream velocity interval for all the tests.

Table 3 Aeronaut 12"x8", 3 bladed Propeller uncertainty for 5000 *RPM* data

	Uncertainty				
V'	V [%]	J [%]	C_T [%]	C_P [%]	η [%]
4	2.834	0.186	0.193	0.463	2.874
5	3.833	0.178	0.173	0.446	3.859
6	2.533	1.744	3.363	3.376	3.126
7	1.480	0.176	0.267	0.502	1.576
8	0.817	0.170	0.245	0.477	0.964
9	0.891	0.166	0.181	0.450	1.003
10	0.551	0.177	0.222	0.520	0.758
11	0.617	0.167	0.236	0.468	0.791
12	0.420	0.163	0.203	0.493	0.660
13	0.334	0.166	0.235	0.540	0.654
14	0.380	0.173	0.332	0.606	0.755
15	0.309	0.171	0.332	0.654	0.765
16	0.376	0.173	0.539	1.407	1.533
17	0.273	0.171	0.926	0.854	1.267

IV. Conclusions

This paper has presented the development and validation of a new test rig, suitable to test a wide range of low Reynolds number propellers up to a diameter of about 14".

Furthermore, the performance of two CAM Carbon Aeronaut propellers was measured over a range of propeller advance ratios for different rotational speeds.

It was shown that as the Reynolds number increases with the increase of propeller *RPM*, the propellers performance is significantly affected by increasing their thrust coefficient and efficiency.

The developed test rig can be used for several purposes, namely to improve the JBLADE Software.

Acknowledgment

The present work was performed as part of Project MAAT (Ref. No. 285602) supported by European Union through the 7th Framework Programme. Part of the work was also supported by C-MAST – Center for Mechanical and Aerospace Sciences and Technologies, Portuguese Foundation for Science and Technology Research Unit No. 151.

References

[1] Z. Zheng, W. Huo, Z. Wu, Autonomous airship path following control: Theory and experiments, *Control Engeneering Practices* Vol. 21, 2013, pp. 769–788.

[2] Q. Wang, J. Chen, G. Fu, D. Duan, An approach for shape optimization of stratosphere airships based on multidisciplinary design optimization, *Journal of*

Zhejiang University Science A. Vol. 10, 2009, pp. 1609–1616.

[3] E.H. van Eaton, Airships and the Modern Military, *U.S. Army War College*, Carlisle Barracks, 1991.

[4] L. Liao, I. Pasternak, A review of airship structural research and development, *Progress in Aerospace Sciences* Vol. 45, No. 4, 2009, pp. 83–96.

[5] J. Morgado, M.Â.R. Silvestre, J.C. Páscoa, Parametric Study of a High Altitude Airship According to the Multi-Body Concept for Advanced Airship Transport - MAAT, in: *IV Conferência Nacional em Mecânica Dos Fluidos, Termodinâmica e Energ*ia, Lisbon, 2012.

[6] Y.-G. Lee, D.-M. Kim, C.-H. Yeom, Development of Korean High Altitude Platform Systems, *International Journal of Wireless and Informatics and Networks*. Vol. 13, 2005, pp. 31–42.

[7] M.S. Smith, E.L. Rainwater, Applications of Scientific Ballooning Technology to High Altitude Airships, in: AIAA's *3rd Annual Aviation Technology Integration Operations and Technology Forum*, Denver, 1971: pp. 1–8.

[8] P. Martin, A. Milan., 2010, Switching Power Supply Unit For An Autonomous Monitoring System, WSEAS TRANSACTIONS on CIRCUITS and SYSTEMS, Issue 10, Vol. 9.

[9] A. Dumas, M. Trancossi, M. Madonia, I. Giuliani, Multibody Advanced Airship for Transport, in: *Society of Automotive Engineers Technical Paper* 2011-01-2786, 2011.

[10] G. Ilieva, J.C. Páscoa, A. Dumas, M. Trancossi, A critical review of propulsion concepts for modern airships, *Central European Journal of Engineering.* Vol. 2, 2012, pp. 189–200.

[11] Lockheed Martin, High Altitude Airship (HAA) *Persistent Communications and ISR for the Joint Warfighter Partnering to Meet Customers' Defining Moments*, Defense.

[12] A. Colozza, B. Park, Initial Feasibility Assessment of a High Altitude Long Endurance Airship, 2003.

[13] A.C. Gawale, R.S. Pant, Initial Sizing and Sensitivity Analyses of Stratospheric Airships for Psuedolite Based Precision Navigation System, in: *5th ATIO and 16th Lighter-Than-Air Systems Technologies and Balloon Systems Conference*, American Institute of Aeronautics and Astronautics, Arlington, 2000, pp. 1–15.

[14] Egrett II Brochure, E-Systems GreenVille Division, 1991

[15] A. Colozza, High Altitude Propeller Design and Analysis Overview, *Technical Report* Cleveland, 1998.

[16] Merlin, P. W., "Crash Course - Lessons Learned from Accidents Involving Remotely Piloted and Autonomous Aircraft", *Monographs in Aerospace History #44*, National Aeronautics and Space Administration, 2013.

[17] M.A. Silvestre, J.P. Morgado, J. Pascoa, JBLADE: a Propeller Design and Analysis Code, *2013 International Powered Lift Conference*, American Institute of Aeronautics and Astronautics, Reston, Virginia, 2013.

[18] J. Morgado, M.A.R. Silvestre, J.C. Páscoa, Validation of New Formulations for Propeller Analysis, Journal of Propulsion and Power. DOI: 10.2514/1.B35240

[19] Drela, M., "XFOIL - An Analysis and Design System for Low Reynolds Number Airfoils", *Proceedings of Low Reynolds Number Aerodynamics*, Berlin, Vol. 54, 1989, pp. 1–12.

[20] Prasetyo Edi, Nukman Yusoff, Aznijar Ahmad Yazid, 2008, The Design Improvement of Airfoil for Flying Wing UAV, WSEAS TRANSACTIONS on APPLIED and THEORETICAL MECHANICS, Issue 9, Vol. 3.

[21] M.S. Selig, Low Reynolds Number Airfoil Design Lecture Notes, *Von Kármán Institute*, 2003.

[22] T. Theodorsen, G.W. Stickle, M.J. Brevoort, Caracteristics of Six Propellers Including the High-Speed Range, *NACA Technical Report No. 594*, Langley, 1937.

[23] W. Gray, Wind-Tunnel Tests of Two Hamilton Standard Propellers Embodying Clark Y and Naca 16-Series Blade Sections, *NACA Technical Report No. 530*, Washington, 1941.

[24] Prasetyo Edi, Khairi Yusuf, Amir Radzi, Abdul Ghani, Hakim S. Sultan Aljibori., 2009, The Design of Light Jet Aircraft, WSEAS TRANSACTIONS on APPLIED and THEORETICAL MECHANICS, Issue 2, Vol. 4.

[25] R.W. Deters, G.K. Ananda, M.S. Selig, Reynolds Number Effects on the Performance of Small-Scale Propellers, *Procedings of 32nd AIAA Applied Aerodynamics Conference, A*merican Institute of Aeronautics and Astronautics, Atlanta, 2014.

[26] J.B. Brandt, M.S. Selig, Propeller Performance Data at Low Reynolds Numbers, (2011) 1–18.

[27] O.R. Shetty, M.S. Selig, Small-Scale Propellers Operating in the Vortex Ring State, in: 49th AIAA Aerosp. Sci. Meet. Incl. New Horizons Forum Aerosp. Expo., Orlando, Florida, 2011: pp. 1–16.

[28] Ananda, G., UIUC Propeller Database, Aerospace Engineering, *University of Illinois Champaign*, IL, http://aerospace.illinois .edu/m-selig/props/propDB.html [retrieved 25 September 2014].

[29] H. Glauert, Wind Tunnel Interference on Wings, Bodies, and Airscrews, 1933.

[30] A. Pope, J. Barlow, W. H. Rae, LOW-SPEED WIND TUNNEL TESTING, 1999.

[31] J.B. Brandt, SMALL-SCALE PROPELLER PERFORMANCE AT LOW SPEEDS, 2005.

[32] M.S. Selig, G. Ananda, Low Reynolds Number Propeller Perfomance Data : Wind Tunnel Corrections for Motor Fixture Drag, 2011.

[33] Hallauer W. L. Jr. and Devenport W. J., 2006, AOE 3054 Experimental Methods Course Manual. Experimental Error, A.O.E. Department, Virginia Tech. Blacksburg VA.